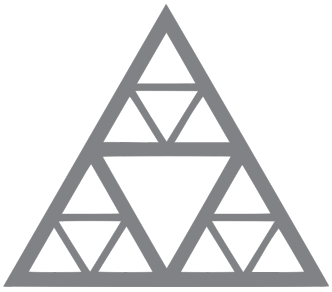

École des Ponts
ParisTech

École des Ponts ParisTech

2023
Rapport de
projet de fin d'études

Zuodong Wang

Élève ingénieur

Testing some advanced numerical methods for hyperbolic, parabolic and elliptic PDEs

(Evaluation de méthodes numériques avancées pour les équations hyperboliques, paraboliques et elliptiques)

Centre Inria de Paris

2 Rue Simone Iff, 75012 Paris

Under the kind supervision of
Zhaonan Dong, Alexandre Ern & Jean-Luc Guermond

Fiche de synthèse

- Type de stage : PFE

- Année : 2023

- Auteur (Nom, prénom) : Wang, Zuodong

- Formation 3ème année: IMI

- Titre du rapport : Testing some advanced numerical methods for hyperbolic, parabolic and elliptic PDEs

- Titre en français: Evaluation de méthodes numériques avancées pour les équations hyperboliques, paraboliques et elliptiques

- Organisme d'accueil : Centre Inria de Paris

- Pays d'accueil : France

- Responsables de stage : Zhaonan Dong, Alexandre Ern & Jean-Luc Guermond

- Mots-clés: lois de conservation, systèmes hyperboliques, problèmes paraboliques, domaine invariant

Synthèse du rapport en français

Ce projet de fin d'études fait partie de ma thèse et s'inscrit dans la continuité de mon stage de master. Mon travail principal au cours de ce projet de fin d'études était de traduire le code en Matlab de Zhaonan Dong à mon module en Python, et de l'enrichir avec des nouvelles fonctionnalités. En particuliar, j'ai réalisé des implémentations numériques afin d'approcher des solutions issues des trois principales classes d'équations aux dérivées partielles. Pour les problèmes hyperboliques, les schémas d'ordre un avaient été implémentés pendant le stage de master, tandis que ce projet de fin d'études a été consacré à l'implémentation de certains schémas d'ordre élevé, ainsi qu'à la résolution de certains détails qui n'avaient pas été pris en compte pendant le stage de master. Pour les problèmes paraboliques, j'ai mis en œuvre un couplage d'éléments finis discontinus en temps et d'éléments finis en espace d'ordre arbitraire. Enfin, pour les problèmes elliptiques, j'ai mis en œuvre des éléments finis continus, des éléments finis discontinus et la méthode hybride high-order (HHO) pour résoudre le problème de Poisson.

A l'issue de ce projet de fin d'études, il y a plus de flexibilité dans la mise en œuvre du code en comparant avec le code issu du stage de master. Alors que le code précédent utilisait les informations de maillage générées par Matlab, maintenant n'importe quel type de maillage supporté par le module meshio en python peut être lu correctement, et il est possible de générer les informations géométriques nécessaires aux calculs ultérieurs. En ce qui concerne l'implémentation des fonctions de base, j'ai actuellement écrit la base de Lagrange, la base de Legendre et quelques autres fonctions de base fréquemment utilisées. En termes d'intégration numérique, les points d'intégration et les poids utilisés pour les éléments finis continus et discontinus n'étaient pas unifiés dans le code de master, mais dans le nouveau code, je les ai unifiés, améliorant ainsi la lisibilité du code.

Pour les problèmes hyperboliques, j'ai principalement résolu certains des problèmes laissés en suspens lors du stage de master, ainsi que la mise en œuvre des méthodes d'ordre élevé. Le code résout maintenant les équations d'Euler correctement en utilisant le schéma d'ordre un. En ce qui concerne le choix des fonctions de base, l'ordre polynomial en espace peut maintenant être arbitrairement élevé, sauf que les exemples numériques d'éléments finis d'ordre élevé ne sont pas présentés dans ce rapport en raison du temps de calcul et de la performance en python encore peu satisfaisante. La discrétisation d'ordre élevé en temps met en œuvre la méthode SSPRK, tandis que la méthode d'ordre élevé en espace est obtenue en réduisant la viscosité et en utilisant la matrice de masse consistante. Pour garantir la préservation du domaine invariant, le limiteur de Boris–Book–Zales est disponible.

Le code pour les problèmes paraboliques a été écrit principalement pour disposer d'une méthode implicite en temps d'ordre élevé. En prenant l'équation de la chaleur comme exemple, j'ai implémenté un couplage d'éléments finis discontinus en temps d'ordre arbitraire et d'éléments finis continus en espace d'ordre arbitraire. En fait, nous pouvons implémenter n'importe quel type de discrétisation spatiale couplée à l'algorithme en temps, mais le développement reste à faire si le besoin se fait sentir.

Pour les problèmes elliptiques, j'ai écrit un certain nombre de méthodes de discrétisation. Étant donné qu'en pratique, lorsque nous traiterons ultérieurement les problèmes spatio-temporels, il nous suffira de considérer comment coupler les algorithmes en temps et les méthodes en espace, nous mettons pour l'instant en œuvre des éléments finis continus, discontinus, et les méthodes HHO.

Contents

Abstract

This internship is the continuation of my master's project. During the past six months, I implemented various numerical methods for hyperbolic, parabolic and elliptic PDEs. For the hyperbolic case, the Euler equations with ideal gas law are realized, and three high-order methods are tested for scalar hyperbolic conservation laws. For the parabolic case, a scheme with arbitrary-order discontinuous Galerkin (dG) method in time and Lagrange finite elements method (FEM or cG method) in space is implemented. Finally, for the elliptic case, the Poisson problem is solved using FEM, dG and hybrid high-order (HHO) methods.

1 Introduction

The mathematical properties of conservation laws and hyperbolic systems are studied in Chapter 1 in [1], [2], pages 1-104 in [9], Chapter 5 in [16], and Chapter 6 in [18]. The existence of shocks and discontinuities for conservation laws and hyperbolic systems is a huge challenge for theoretical and numerical investigations. Indeed, even if the initial datum is smooth, it is possible to observe a shock during the time evolution. Therefore, one should interpret the solution in a weak sense instead of a strong sense. These weak solutions are merely bounded locally in space and in time. A reasonable weak solution should be a solution which correctly represents the physical properties. This is usually done by requiring the satisfaction of an entropy condition whenever there are entropies associated with the conservation law or the hyperbolic system. A huge body of literature is devoted to the numerical approximation of conservation laws and hyperbolic systems. For instance, [4, 5] studies the convergence to the entropy weak solution for scalar problems with the finite volume method, and the continuous/discontinuous Galerkin method is investigated in [12, 17]. This report focuses on the numerical realization of an invariant-domain-preserving (IDP) scheme, and its high-order extension designed in [10] and [14]. An overview can be found in Chapters 81, 82 and 83 in [7].

Moreover, my PhD program also focuses on degenerate parabolic problems, so parabolic problems and elliptic problems have also been implemented during this internship.

The report is organized as follows: In Section 2, we solve the Euler equations with ideal gas law by a first-order scheme, and scalar conservation laws are solved by various high-order schemes. In Section 3, we solve the heat equation by using dG for temporal discretization and cG for spatial discretization. Finally, in Section 4, we solve the elliptic problem by cG, dG and HHO.

We denote d the space dimension, Ω an open polyhedral domain in $\mathbb{R}^d$, and T the final time.

2 Hyperbolic case

During my master's internship, we proved the convergence of the low-order invariant-domain-preserving (IDP) scheme proposed in [10] and [14], under some mild assumptions on the numerical solution. At the same time, we illustrated our theoretical results by means of numerical experiments using a low-order scheme. However, we did not implement the low-order scheme for Euler equations and we did not implement high-order schemes. This section presents numerical results in these cases.

In general, we aim at solving the following problem with suitable initial conditions, boundary conditions and entropy conditions:

$$\partial_t \boldsymbol{u} + \nabla \cdot \mathbb{f}(\boldsymbol{u}) = 0, \ \forall (x,t) \in \Omega \times (0,T), \tag{1}$$

where $\boldsymbol{u}$ has m components, $\boldsymbol{u}$ stays in an invariant convex set $\mathcal{B}$ for a.e. $(x,t) \in \Omega \times (0,T)$, $\mathbb{f} \in W^{1,\infty}(\mathcal{B}; \mathbb{R}^{m\times d})$.

For the low-order spatial discretization, the P_1 Lagrange finite elements are used. The low-order numerical scheme used in this report has the form

$$m_i \frac{\boldsymbol{U}_i^{n+1} - \boldsymbol{U}_i^n}{\tau} + \sum_{j \in \mathcal{I}(i)\setminus\{i\}} \Big(\mathbb{f}(\boldsymbol{U}_j^n)\boldsymbol{c}_{ij} + d_{ij}^n (\boldsymbol{U}_i^n - \boldsymbol{U}_j^n) \Big) = 0, \tag{2}$$

for all degrees of freedom i. A more detailed description can be found in Chapters 81 in [7] where the same notation is used.

We use a strong stability-preserving Runge–Kutta (SSPRK) scheme for high-order time discretization. In particular, SSPRK(2,2) is tested in our numerical experiments. The high-order viscosity considered in this work is either a

smoothness-based graph viscosity, or a greedy graph viscosity and or an entropy-based graph viscosity. The numerical tests for entropy-based graph viscosity use the consistent mass matrix and the Boris–Book–Zalesak (BBZ) limiting technique. Details on these methods can be found in Chapters 82 and 83 in [7]. In addition, for the smoothness-based graph viscosity, the CFL constant is set to 1, for greedy graph viscosity and entropy-based graph viscosity, the CFL constant is set to 0.25.

2.1 Euler equations

We consider the compressible Euler equations in conservative form:

$$\begin{cases} \rho_t + \nabla\cdot\boldsymbol{m} = 0, \\ \boldsymbol{m}_t + \nabla\cdot(\boldsymbol{v}\otimes\boldsymbol{m}) + \nabla p = 0, \\ E_t + \nabla\cdot(\boldsymbol{v}(E+p)) = 0, \end{cases}$$

with initial conditions, proper boundary conditions and the equation of state. In this report, we consider an ideal gas where the equation of state is $p = (\gamma-1)\rho e,\ e = \rho^{-1}E - \frac{\boldsymbol{m}^2}{2\rho^2}$, where the heat capacity ratio γ is in the range $(1, \frac{5}{3}]$.

For estimating the maximum wave speed, we use the algorithm proposed in [13]. The examples tested in this subsection are from [11]. I did not yet implement the high-order scheme for the system case, so all the numerical experiments presented herein are realized by the low-order method.

2.1.1 One-dimensional smooth wave

This example is from Section 5.2 in [11]. The solution in this example is sufficiently smooth for observing first-order convergence. The error is defined as the sum of the relative error of all components. The convergence results are reported in Table 1.

Table 1: One-dimensional smooth wave

	L^1		L^2		L^∞	
DoFs	error	rate	error	rate	error	rate
128×3	1.69E-01	-	3.26E-01	-	7.19E-01	-
256×3	1.28E-01	0.40	2.59E-01	0.33	5.71E-01	0.33
512×3	8.69E-02	0.56	1.84E-01	0.48	4.07E-01	0.49
1024×3	5.32E-02	0.70	1.18E-01	0.65	2.56E-01	0.67

2.1.2 Leblanc shocktube

The construction of the exact solution is given in Section 5.4 of [11], and the final time is $T = 2/3$. The convergence results for the relative error on density are reported in Table 2.

Table 2: Leblanc shocktube

	L^1		L^2		L^∞	
DoFs	error	rate	error	rate	error	rate
100×3	4.67E-02	-	4.71E-02	-	8.93E-02	-
200×3	3.54E-02	0.40	3.42E-02	0.45	6.70E-02	0.41
400×3	2.56E-02	0.47	2.50E-02	0.45	5.09E-02	0.40
800×3	1.77E-02	0.53	1.83E-02	0.44	3.75E-02	0.44

The numerical solution (with blue color) and the exact solution (with orange color) with 2^{11} DoFs are plotted in Figure 1, where the small shock is rather well captured by the scheme.

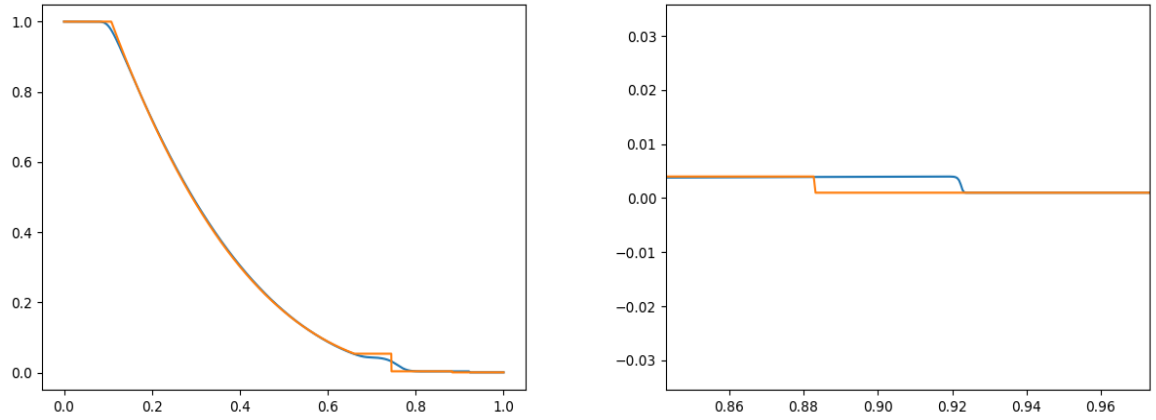

(a) Simulated and exact solutions

(b) Zoom around the small shock

Figure 1: Numerical simulation for Leblanc shocktube

2.1.3 Sod, Lax and Woodward-Collela waves

We illustrate some benchmark examples in Figure 2 where the solutions are similar to those in [11]. The detailed descriptions can be found in Section 5.5 in [11].

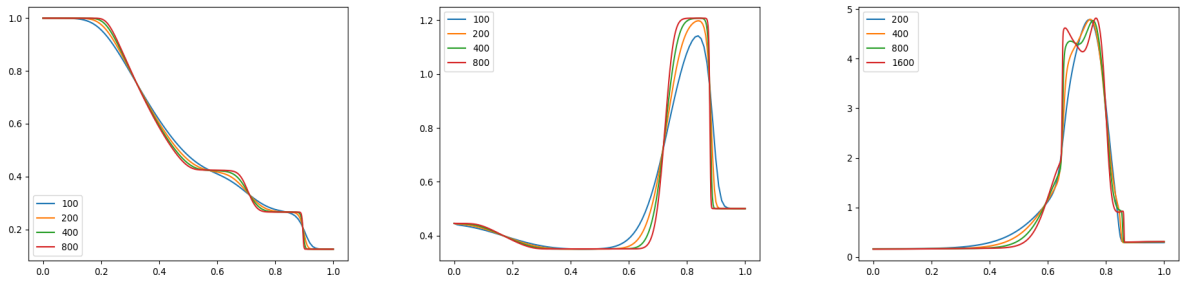

(a) Sod shocktube

(b) Lax shocktube

(c) Woodward-Collela blast

Figure 2: Numerical simulation for benchmark examples using meshes with increasing refinement

2.1.4 Two-dimensional isentropic vortex

This smooth example is from Section 5.6 of [11], but the final time in my test is $T = 0.2$ in order to save some computational time. The relative energy error is reported in Table 3.

Table 3: Two-dimensional isentropic vortex

	L^1		L^2		L^∞	
DoFs	error	rate	error	rate	error	rate
30×4	1.05E-02	-	4.52E-02	-	4.91E-01	-
101×4	6.09E-03	0.90	2.64E-02	0.89	3.29E-01	0.65
369×4	4.41E-03	0.49	2.39E-02	0.15	3.17E-01	0.06
1409×4	2.42E-03	0.89	1.39E-02	0.81	1.91E-01	0.76
5505×4	1.42E-03	0.79	8.44E-03	0.74	1.17E-01	0.72
21761×4	7.59E-04	0.91	4.61E-03	0.88	0.64E-02	0.86

2.2 Linear transport with smooth solution in 1D

This example is from section 4.3.1 of [8]. The initial data is $u_0(x) = (4\frac{(x-0.1)(0.4-x)}{0.3})^6$, the final time is $T = 0.2$, the domain is $\Omega = (-1, 1)$, and the maximum wave speed is $\lambda_{\max} = 1$. The relative error is reported in Tables 4, 5, and 6, along with convergence rates for various choices of the high-order graph viscosity.

Table 4: Linear transport in 1D with smoothness-based graph viscosity

	L^1		L^2		L^∞	
DoFs	error	rate	error	rate	error	rate
64	4.91E-01	-	3.96E-01	-	3.98E-01	-
128	1.73E-01	1.50	1.63E-01	1.28	1.88E-01	1.08
256	6.10E-02	1.51	6.07E-02	1.43	7.67E-02	1.29
512	1.76E-02	1.79	1.84E-02	1.71	2.98E-02	1.36
1024	4.67E-03	1.91	5.38E-03	1.77	1.12E-03	1.41

Table 5: Linear transport in 1D with greedy graph viscosity

	L^1		L^2		L^∞	
DoFs	error	rate	error	rate	error	rate
64	3.64E-01	-	3.11E-01	-	3.13E-01	-
128	1.28E-01	1.51	1.16E-01	1.42	1.27E-01	1.30
256	4.64E-02	1.46	4.26E-02	1.44	5.08E-02	1.32
512	1.40E-02	1.73	1.31E-02	1.70	1.90E-02	1.42
1024	3.86E-03	1.85	3.96E-03	1.72	8.93E-03	1.08

Table 6: Linear transport in 1D with entropy-based graph viscosity

	L^1		L^2		L^∞	
DoFs	error	rate	error	rate	error	rate
64	3.24E-01	-	2.55E-01	-	2.71E-01	-
128	6.83E-02	2.25	5.70E-02	2.16	7.68E-02	1.82
256	1.30E-02	2.40	1.01E-02	2.43	1.04E-02	2.88
512	1.92E-03	2.75	1.82E-03	2.53	2.86E-03	1.87
1024	3.01E-04	2.68	3.47E-04	2.39	8.59E-04	1.73

Then, simulated solutions at final time are plotted in Figure 3.

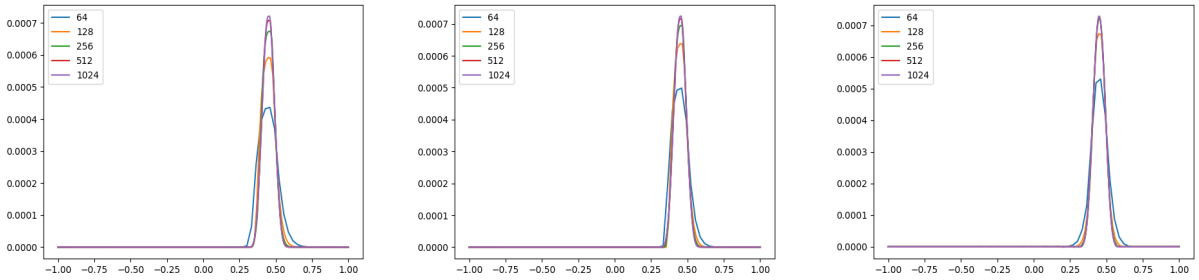

(a) Smoothness-based viscosity (b) Greedy graph viscosity (c) Entropy-based graph viscosity

Figure 3: Linear transport in 1D: solutions at final time for meshes with increasing refinement

2.3 Linear transport with smooth solution in 2D

The test example is from Section 4.3.2 of [8] with $x_0 = y_0 = -0.8$, $x_1 = y_1 = 0.2$. The final time is $T = 0.5$, and the maximum wave speed is $\lambda_{\max} = 1.5$. (This value is a bit larger than the guaranteed upper bound). The convergence results are reported in Tables 7, 8, and 9.

Table 7: Linear transport in 2D with low-order method

	L^1		L^2		L^∞	
DoFs	error	rate	error	rate	error	rate
129	1.23E-00	-	7.97E-01	-	8.41E-01	-
481	9.52E-01	0.39	6.51E-01	0.31	7.14E-01	0.25
1857	6.45E-01	0.54	4.77E-01	0.46	5.45E-01	0.40
7297	3.96E-01	0.71	3.12E-01	0.62	3.67E-01	0.58

Table 8: Linear transport in 2D with entropy-based graph viscosity ($\eta(u) = 0.5u^2$)

	L^1		L^2		L^∞	
DoFs	error	rate	error	rate	error	rate
129	7.72E-01	-	5.43E-01	-	6.11E-01	-
481	2.86E-01	1.51	1.99E-01	1.53	2.19E-01	1.56
1857	6.99E-02	2.09	4.58E-02	2.17	5.36E-02	2.08
7297	1.31E-02	2.45	8.99E-03	2.38	1.62E-02	1.75

Table 9: Linear transport in 2D with greedy viscosity

	L^1		L^2		L^∞	
DoFs	error	rate	error	rate	error	rate
129	7.53E-01	-	5.77E-01	-	6.59E-01	-
481	2.54E-01	1.65	2.40E-01	1.33	3.28E-01	1.06
1857	9.32E-02	1.48	8.30E-02	1.57	1.25E-01	1.43
7297	2.60E-02	1.87	2.20E-02	1.94	4.54E-02	1.48
28929	6.54E-03	2.00	5.49E-03	2.01	1.62E-02	1.49

2.4 Burgers' equation with shock in 2D

The example tested is from [15], the maximum wave speed is $\lambda_{\max} = 1$. The convergence results are reported in Tables 10, 11, 12, and 13. We observe that using a strictly convex entropy performs better than using a non-strictly convex entropy.

Table 10: Burgers' equation with low-order method

	L^1		L^2		L^∞	
DoFs	error	rate	error	rate	error	rate
12	6.98E-01	-	9.71E-01	-	1.69E-00	-
37	5.94E-01	0.29	8.43E-01	0.25	1.66E-00	0.03
129	4.18E-01	0.56	6.09E-01	0.52	1.66E-00	0.00
481	2.88E-01	0.56	4.35E-01	0.52	1.64E-00	0.02
1857	1.87E-01	0.64	3.17E-01	0.47	1.73E-00	0.08

Table 11: Burgers' equation with entropy-based graph viscosity ($\eta(u) = |u - k|$)

	L^1		L^2		L^∞	
DoFs	error	rate	error	rate	error	rate
12	7.31E-01	-	1.05E-00	-	1.71E-00	-
37	6.13E-01	0.31	8.75E-01	0.32	1.68E-00	0.03
129	3.77E-01	0.78	5.44E-01	0.72	1.66E-00	0.02
481	2.68E-01	0.52	4.11E-01	0.42	1.65E-00	0.01
1857	1.76E-01	0.62	3.02E-01	0.46	1.74E-00	-0.07

Table 12: Burgers' equation with entropy-based graph viscosity ($\eta(u) = 0.5u^2$)

	L^1		L^2		L^∞	
DoFs	error	rate	error	rate	error	rate
12	6.96E-01	-	9.61E-01	-	1.65E-00	-
37	5.70E-01	0.35	8.06E-01	0.31	1.63E-00	0.02
129	3.54E-01	0.76	5.12E-01	0.73	1.61E-00	0.01
481	2.26E-01	0.68	3.61E-01	0.53	1.63E-00	0.01
1857	1.22E-01	0.92	2.51E-01	0.54	1.74E-00	-0.1

Table 13: Burgers' equation with greedy viscosity

	L^1		L^2		L^∞	
DoFs	error	rate	error	rate	error	rate
12	5.96E-01	-	8.48E-01	-	1.55E-00	-
37	3.91E-01	0.75	6.68E-01	0.42	1.58E-00	-0.04
129	2.67E-01	0.61	4.33E-01	0.69	1.70E-00	-0.11
481	1.57E-01	0.81	2.81E-01	0.66	1.65E-00	0.05
1857	9.80E-02	0.70	2.05E-01	0.47	1.74E-00	0.08

2.5 Non-strictly convex flux

This test is designed to show that we should take the entropy information into account for the design of the scheme, since high-order schemes may violate the entropy condition. Here, we consider the Riemann problem with the flux

$$f(u) = \begin{cases} 2-u, & \text{if } u \le 2, \\ 2u-4, & \text{otherwise.} \end{cases}$$

The exact solution is such that

$$u(x,t) = \begin{cases} 1, & \text{if } x \le -t, \\ 2, & \text{if } -t < x \le 2t, \\ 3, & \text{otherwise.} \end{cases}$$

The final time is $T = 0.5$, the domain is $\Omega = (-1, 1)$ and the maximum wave speed is $\lambda_{max} = 2$. The convergence results are reported in Tables 14, 15, and 16.

Table 14: Low-order method for non-strictly convex flux

	L^1		L^2		L^∞	
DoFs	error	rate	error	rate	error	rate
16	9.08E-02	-	1.17E-01	-	1.90E-01	-
32	6.29E-02	0.53	9.43E-02	0.31	1.84E-01	0.04
64	4.40E-02	0.51	7.78E-02	0.28	1.80E-01	0.03
128	3.10E-02	0.51	6.48E-02	0.26	1.76E-01	0.03
256	2.19E-02	0.50	5.41E-02	0.26	1.73E-01	0.02

Table 15: Non-strictly convex flux with greedy graph viscosity

	L^1		L^2		L^∞	
DoFs	error	rate	error	rate	error	rate
16	9.98E-02	-	1.48E-01	-	2.75E-01	-
32	5.96E-02	0.74	1.11E-01	0.42	2.69E-01	0.03
64	3.09E-02	0.95	8.00E-02	0.47	2.67E-01	0.01
128	1.62E-02	0.92	5.76E-02	0.47	2.62E-01	0.03
256	8.75E-03	0.89	4.17E-02	0.47	2.55E-01	0.04

Table 16: Non-strictly convex flux with entropy-based graph viscosity ($\eta(u) = 0.5u^2$)

	L^1		L^2		L^∞	
DoFs	error	rate	error	rate	error	rate
16	5.15E-02	-	8.28E-02	-	1.92E-01	-
32	2.65E-02	0.96	5.83E-02	0.50	1.83E-01	0.01
64	1.42E-02	0.90	4.22E-02	0.47	1.81E-01	0.02
128	7.96E-03	0.84	3.14E-02	0.43	1.78E-01	0.00
256	4.68E-03	0.77	2.43E-02	0.37	1.91E-01	-0.10

The simulated solutions with low-order method, entropy-based and greedy graph viscosity are plotted at the final time $T = 0.25$ in Figure 4. We observe that the greedy graph viscosity is entropy-violating.

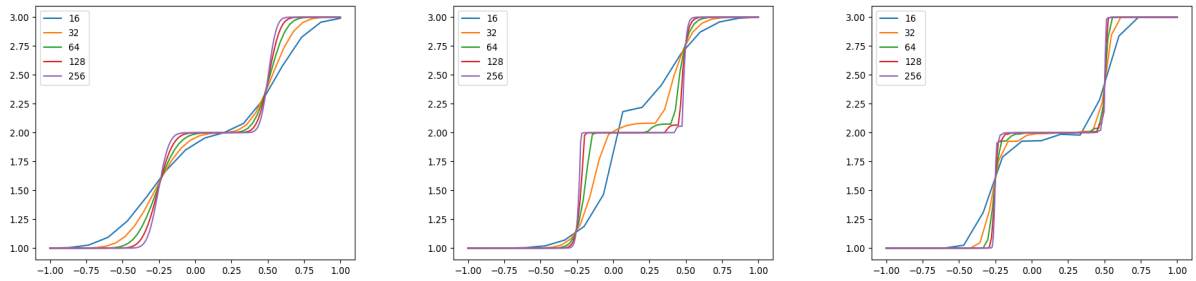

(a) Low-order viscosity (b) Greedy graph viscosity (c) Entropy-based graph viscosity

Figure 4: Simulated solutions for non-strictly convex flux on meshes with increasing refinement

3 Parabolic case

The second part of this internship is to prepare the implementation for degenerate parabolic problems. For the moment, I implemented discretization schemes for the heat equation with arbitrary-order Lagrange FEM for space discretization and arbitrary-order dG in time with a Legendre basis.

The equation tested in this section is

$$\partial_t u - \Delta u = f, \ \forall (x,t) \in \Omega \times (0,T],$$

with $\Omega = (-1,1)^2$, $T = 1$, and Dirichlet boundary conditions over the whole boundary. The exact solution is $u(x,t) = \sin(x_1)\sin(x_2)\exp(t)$.

For brevity, we only present the convergence results for P_2 Lagrange FEM in space and 3rd-order dG in time. In Table 17, relative errors are measured in the $L^\infty(L^2)$- and $L^2(H_0^1)$-norms. We observe the expected convergence rates.

Table 17: Heat equation in 2D

	$L^2(H_0^1)$		$L^\infty(L^2)$	
DoFs	error	rate	error	rate
37	4.62E-02	-	1.83E-02	-
129	1.11E-02	2.28	1.60E-03	3.90
481	2.76E-03	2.11	2.01E-04	3.15
1857	6.91E-04	2.05	2.62E-05	3.01
7297	1.73E-04	2.03	3.18E-06	3.08

4 Elliptic case

In this section, we focus on the Poisson problem with various spatial discretizations. The PDE model considered here is

$$-\Delta u = f, \ \forall x \in \Omega,$$

with $\Omega = (-1, 1)^2$ and Dirichlet boundary conditions over the whole boundary. The exact solution is $u(x) = \sin(x_1)\sin(x_2)$.

4.1 Lagrange finite elements

Lagrange finite elements with arbitrary-order are implemented. For brevity, we only present in Tables 18 and 19 the relative error in the L^2- and H_0^1-norms with polynomial degrees equal to 1 and 5.

Table 18: Lagrange FEM P_1 for Poisson problem

	H_0^1		L^2	
DoFs	error	rate	error	rate
12	3.73E-01	-	1.16E-01	-
37	1.93E-01	1.17	3.11E-02	2.34
129	9.71E-01	1.01	7.78E-03	2.22
481	4.86E-01	1.05	1.95E-03	2.10

Table 19: Lagrange FEM P_5 for Poisson problem

	H_0^1		L^2	
DoFs	error	rate	error	rate
197	1.20E-05	-	1.38E-06	-
741	3.89E-07	5.16	2.20E-08	6.22
2881	1.19E-08	5.13	3.36E-10	6.16
11361	3.75E-10	5.04	5.32E-12	6.05

4.2 Dubiner Finite elements

Here, our numerical experiments are realized with the Dubiner basis. We present in Tables 20 and 21 the relative error in the L^2- and H_0^1- norms with polynomial degrees equal to 2 and 3.

Table 20: P_2 FEM with Dubiner basis for Poisson problem

	H_0^1		L^2	
DoFs	error	rate	error	rate
37	4.61E-02	-	1.41E-02	-
129	1.11E-02	2.28	1.54E-03	3.55
481	2.76E-02	2.11	1.86E-04	3.21
1857	6.92E-04	2.05	2.30E-05	3.10

Table 21: P_3 FEM with Dubiner basis for Poisson problem

	H_0^1		L^2	
DoFs	error	rate	error	rate
76	3.57E-03	-	6.12E-04	-
277	4.70E-04	3.14	4.06E-05	4.19
1057	5.85E-05	3.11	2.53E-06	4.15
4129	7.35E-06	3.05	1.58E-07	4.07

4.3 Discontinuous Galerkin method

There are many different dG methods for solving the Poisson problems. The Symmetric Interior Penalty (SIP) method is used in our numerical experiments. Details about the SIP method can be found in Chapter 4 in [6].

The relative errors in the L^2- and H_0^1-norms with Legendre basis of order 1 and 4 are reported in Tables 22 and 23.

Table 22: P_1 dG for Poisson problem

	H_0^1		L^2	
DoFs	error	rate	error	rate
42	2.57E-01	-	6.11E-02	-
168	1.34E-01	0.95	1.59E-02	1.94
672	6.73E-02	0.99	3.87E-03	2.00
2688	3.37E-02	1.00	9.95E-04	2.00

Table 23: P_4 dG for Poisson problem

	H_0^1		L^2	
DoFs	error	rate	error	rate
210	2.67E-04	-	5.08E-05	-
840	1.51E-05	4.14	1.43E-06	5.15
3360	9.39E-07	4.01	4.53E-08	4.98
13440	5.87E-08	4.00	1.44E-09	4.97

4.4 Hybrid high-order method

For the implementation of the HHO method, the Legendre basis is used for both cell basis and face basis functions. The cell basis functions are one order higher than the face basis functions. The details on the HHO method can be found in Chapter 1 and Section 3.2 in [3].

The relative error in the L^2- and H_0^1-norms with Legendre basis of order 0 and 1 for the face basis functions are reported in Tables 24 and 25.

Table 24: HHO with constant basis on faces for Poisson problem

	H_0^1		L^2	
DoFs on face	error	rate	error	rate
25	2.93E-01	-	1.71E-01	-
92	1.60E-01	0.92	5.07E-02	1.86
352	8.20E-02	1.00	1.31E-02	2.02
1376	4.12E-02	1.00	3.30E-03	2.02

Table 25: HHO with affine basis on faces for Poisson problem

	H_0^1		L^2	
DoFs on face	error	rate	error	rate
50	4.02E-02	-	1.02E-02	-
185	9.68E-03	2.18	1.18E-03	3.31
704	2.41E-03	2.07	1.44E-04	3.15
2752	6.01E-04	2.04	1.77E-05	3.07

References

[1] F. BOUCHUT, *Nonlinear stability of finite volume methods for hyperbolic conservation laws and well-balanced schemes for sources*, Frontiers in Mathematics, Birkhäuser Verlag, Basel, 2004.

[2] A. BRESSAN, *Hyperbolic conservation laws: an illustrated tutorial*, in Modelling and optimisation of flows on networks, vol. 2062 of Lecture Notes in Math., Springer, Heidelberg, 2013, pp. 157–245.

[3] M. CICUTTIN, A. ERN, AND N. PIGNET, *Hybrid high-order methods—a primer with applications to solid mechanics*, SpringerBriefs in Mathematics, Springer, Cham, [2021] ©2021.

[4] B. COCKBURN, F. COQUEL, AND P. G. LEFLOCH, *Convergence of the finite volume method for multidimensional conservation laws*, SIAM J. Numer. Anal., 32 (1995), pp. 687–705.

[5] M. G. CRANDALL AND A. MAJDA, *Monotone difference approximations for scalar conservation laws*, Math. Comp., 34 (1980), pp. 1–21.

[6] D. A. DI PIETRO AND A. ERN, *Mathematical aspects of discontinuous Galerkin methods*, vol. 69 of Mathématiques & Applications (Berlin) [Mathematics & Applications], Springer, Heidelberg, 2012.

[7] A. ERN AND J.-L. GUERMOND, *Finite elements III—first-order and time-dependent PDEs*, vol. 74 of Texts in Applied Mathematics, Springer, Cham, [2021] ©2021.

[8] ——, *Invariant-domain-preserving high-order time stepping: I. Explicit Runge-Kutta schemes*. working paper or preprint, June 2022.

[9] E. GODLEWSKI AND P.-A. RAVIART, *Numerical approximation of hyperbolic systems of conservation laws*, vol. 118 of Applied Mathematical Sciences, Springer-Verlag, New York, 1996.

[10] J.-L. GUERMOND AND M. NAZAROV, *A maximum-principle preserving C^0 finite element method for scalar conservation equations*, Comput. Methods Appl. Mech. Engrg., 272 (2014), pp. 198–213.

[11] J.-L. GUERMOND, M. NAZAROV, B. POPOV, AND I. TOMAS, *Second-order invariant domain preserving approximation of the Euler equations using convex limiting*, SIAM J. Sci. Comput., 40 (2018), pp. A3211–A3239.

[12] J.-L. GUERMOND AND B. POPOV, *Error estimates of a first-order Lagrange finite element technique for nonlinear scalar conservation equations*, SIAM J. Numer. Anal., 54 (2016), pp. 57–85.

[13] ——, *Fast estimation from above of the maximum wave speed in the Riemann problem for the Euler equations*, J. Comput. Phys., 321 (2016), pp. 908–926.

[14] ——, *Invariant domains and first-order continuous finite element approximation for hyperbolic systems*, SIAM J. Numer. Anal., 54 (2016), pp. 2466–2489.

[15] ——, *Invariant domains and second-order continuous finite element approximation for scalar conservation equations*, SIAM J. Numer. Anal., 55 (2017), pp. 3120–3146.

[16] H. HOLDEN AND N. H. RISEBRO, *Front tracking for hyperbolic conservation laws*, vol. 152 of Applied Mathematical Sciences, Springer, Heidelberg, second ed., 2015.

[17] J. JAFFRÉ, C. JOHNSON, AND A. SZEPESSY, *Convergence of the discontinuous Galerkin finite element method for hyperbolic conservation laws*, Math. Models Methods Appl. Sci., 5 (1995), pp. 367–386.

[18] P. G. LEFLOCH, *Hyperbolic systems of conservation laws*, Lectures in Mathematics ETH Zürich, Birkhäuser Verlag, Basel, 2002. The theory of classical and nonclassical shock waves.